



## RESEARCH ARTICLE

# *In silico* screening of known small molecules to bind ACE2 specific RBD on Spike glycoprotein of SARS-CoV-2 for repurposing against COVID-19 [version 1; peer review: 2 approved]

Bharath BR <sup>1</sup>, Hrishikesh Damle<sup>2</sup>, Shiban Ganju<sup>2</sup>, Latha Damle<sup>1</sup>

<sup>1</sup>Computational Biology, Atrimed Biotech LLP, Bangalore, 560100, India

<sup>2</sup>Atrimed Pharmaceuticals Pvt. Ltd, Bangalore, 560001, India

**V1** First published: 01 Jul 2020, 9:663  
<https://doi.org/10.12688/f1000research.24143.1>

Latest published: 01 Jul 2020, 9:663  
<https://doi.org/10.12688/f1000research.24143.1>

## Abstract

**Background:** Human coronavirus (SARS-CoV-2) is causing a pandemic with significant morbidity and mortality. As no effective novel drugs are available currently, drug repurposing is an alternative intervention strategy. Here we present an *in silico* drug repurposing study that implements successful concepts of computer-aided drug design (CADD) technology for repurposing known drugs to interfere with viral cellular entry via the spike glycoprotein (SARS-CoV-2-S), which mediates host cell entry via the hACE2 receptor.

**Methods:** A total of 4015 known and approved small molecules were screened for interaction with SARS-CoV-2-S through docking studies and 15 lead molecules were shortlisted. Additionally, streptomycin, ciprofloxacin, and glycyrrhizic acid (GA) were selected based on their reported anti-viral activity, safety, availability and affordability. The 18 molecules were subjected to molecular dynamics (MD) simulation.

**Results:** The MD simulation results indicate that GA of plant origin may be repurposed for SARS-CoV-2 intervention, pending further studies.



**Conclusions:** Repurposing is a beneficial strategy for treating COVID-19 with existing drugs. It is aimed at using docking studies to screen molecules for clinical application and investigating their efficacy in inhibiting SARS-CoV-2-S. SARS-CoV-2-S is a key pathogenic protein that mediates pathogen-host interaction. Hence, the molecules screened for inhibitory properties against SARS-CoV-2-S can be clinically used to treat COVID-19 since the safety profile is already known.

## Keywords

SARS-CoV-2, Pathogen host interaction, SARS-CoV-2-Spike Glycoprotein, ACE2, Small Molecules

## Open Peer Review

Reviewer Status  

|                          | Invited Reviewers  |  |
|--------------------------|--|--|
|                          | 1  | 2  |
| version 1<br>01 Jul 2020 | <br>report | <br>report |

1 **S.M. Vidya**, NMAM Institute of Technology, Udupi, India

2 **Raghavendra HL** , Wollega University, Nekemte, Ethiopia

Any reports and responses or comments on the article can be found at the end of the article.

**Corresponding author:** Bharath BR ([bharath.br@atrimed.com](mailto:bharath.br@atrimed.com))

**Author roles:** **BR B:** Conceptualization, Investigation, Methodology, Project Administration, Software, Supervision, Visualization, Writing – Original Draft Preparation, Writing – Review & Editing; **Damle H:** Conceptualization, Formal Analysis, Investigation, Supervision, Writing – Review & Editing; **Ganju S:** Conceptualization, Writing – Review & Editing; **Damle L:** Conceptualization, Writing – Review & Editing

**Competing interests:** Latha Damle is the founder of Atrimed Biotech LLP and holds equity in Atrimed Pharmaceuticals. Shiban Ganju and Hrishikesh Damle hold equity shares in Atrimed Pharmaceuticals.

**Grant information:** The study was sponsored by Atrimed Pharmaceuticals Pvt. Ltd and no external funding was received for the study. *The funders had no role in study design, data collection and analysis, decision to publish, or preparation of the manuscript.*

**Copyright:** © 2020 BR B *et al.* This is an open access article distributed under the terms of the [Creative Commons Attribution License](#), which permits unrestricted use, distribution, and reproduction in any medium, provided the original work is properly cited.

**How to cite this article:** BR B, Damle H, Ganju S and Damle L. ***In silico* screening of known small molecules to bind ACE2 specific RBD on Spike glycoprotein of SARS-CoV-2 for repurposing against COVID-19 [version 1; peer review: 2 approved]** F1000Research 2020, 9:663 <https://doi.org/10.12688/f1000research.24143.1>

**First published:** 01 Jul 2020, 9:663 <https://doi.org/10.12688/f1000research.24143.1>

## Introduction

The complete genome of severe acute respiratory syndrome coronavirus 2 (SARS-CoV-2) is 82% identical to SARS-CoV, both viruses share a common clade encompassing the genus *Betacoronavirus* as the root node<sup>1,2</sup>. Currently no novel antivirals exist that are effective against either of the viruses<sup>3-6</sup>.

Drug repurposing is a commercially viable strategy, as it exploits existing drugs, thus significantly reducing the cost and time involved in developing effective therapeutics<sup>7-9</sup>. Experimental approaches, however, at pre-clinical and clinical stages for drug repurposing involve high cost and time<sup>10</sup>. Computational approaches can offer quick, considerable, and novel testable hypotheses for systematic drug repositioning<sup>8</sup>.

Current drugs in different phases of clinical trials are being investigated for inhibitory activity against viral targets that play a significant role in the coronavirus infection lifecycle. The drug targets might be involved in entry into the host (e.g. umifenovir and chloroquine), replication (e.g. lopinavir/ritonavir), or RNA synthesis (e.g. remdesivir/favipiravir). Among these, targeting SARS-CoV-2 cellular entry via the spike glycoprotein (SARS-CoV-2-S) has emerged as the leading option for repurposing<sup>9</sup>. As SARS-CoV-2-S is a surface protein involved in adhesion/fusion and entry into host cells, it has been identified as a potential drug target for both biologics and small molecules<sup>10</sup>.

The entry of COVID-19 pathogen is mediated by the homotrimeric transmembrane protein SARS-CoV-2-S. It is comprised of two functional subunits, S1 and S2, which are non-covalently bound in the pre-fusion conformation. The S1 subunit interacts with the human ACE2 receptor through the receptor binding domain (RBD), while the S2 subunit is one of the components of viral envelope<sup>11-19</sup>.

Apart from interacting with the ACE2 receptor, the RBD site also contributes to the stabilisation of the prefusion state of the S2 subunit equipped with fusion machinery<sup>18-24</sup>. In CoVs, the S-protein is cleaved by host proteases at the S20 site located above the fusion peptide<sup>16,25</sup>. This activates the protein via extensive irreversible conformational changes<sup>11,16,17,23,26</sup>. It is well understood that the entry of CoV into the susceptible host is a complex process that requires the vigorous actions of receptor binding and proteolytic processing of the S-protein to promote fusion with the pathogen<sup>27</sup>.

Hence, the current study aims to predict and validate the structure of SARS-CoV-2-S protein using computer-aided homology modelling tools and screen a library of small molecules for their interaction with the SARS-CoV-2-S protein.

## Methods

### Sequence analysis

The whole genome of SARS-CoV-2 (GenBank accession number: [MT159721.1](#), length: 29882 bp) was retrieved from NCBI and used as a query to perform a sequence similarity search using NCBI-BLAST<sup>28</sup>. The BLAST search revealed 96.04%,

91.64% and 82.30% identity with Bat coronavirus RaTG13 (GenBank accession number: [MN996532.1](#), length: 29855 bp), Pangolin coronavirus isolate MP789 (GenBank accession number: [MT084071.1](#), length: 27213 bp) and SARS-CoV (GenBank accession number: [JX163927](#), length: 29646bp), respectively.

### Topological analysis of pathogen-host interactome for target validation

Drug target identification and validation were carried out using a network-based topological analysis method using the web-based application [Pathogen-Host Interaction Search Tool \(PHISTO\)](#) by setting pathogen type to virus, family to coronaviridae, species to SARS-Related coronavirus and strain to SARS-Cov. The node properties like the degree of connectivity (k) and betweenness centrality (BC) were assessed<sup>29,30</sup>. The statistical significance of k and BC values were assessed by the Fligner-Killeen (median) test.

### Prediction of ligand binding site

The similarity between RBD domains of S-protein from SARS-CoV-2 (accession number [QII57328](#), length:1273aa), SARS-CoV (accession number: [AFR58728](#), length:1255aa) and RatG13 (accession number: [QHR63300](#), length:1269aa) was evaluated by using the multiple sequence alignment (MSA) tool [Clustal Omega](#) from EMBL-EBI. Conservation in ACE2 receptor interaction was seen among all the three sequences aligned. This conservation aided in the active binding site prediction.

The protein-protein interaction between SARS-CoV-2-S and host ACE2 receptor complex was studied using the crystal structure from Protein Data Bank (PDB ID: [6CS2](#)). The amino acids involved in the interaction were identified as ligand binding sites for inhibitor molecules.

### Homology modelling of SARS-CoV-2-S protein

Homology modelling was performed with SWISS-MODEL for the protein sequence of SARS-CoV-2-S using the crystal structure of SARS-CoV-S and ACE2 complex (PDB ID: [6ACD](#)) as a template. The modelled protein was validated for quality using a Ramachandran plot and prepared for molecular docking studies using the Protein Preparation Wizard feature of the Schrodinger Small Molecule Suite<sup>31</sup>. This analysis could also have been performed using open source software such as AutoDock<sup>32</sup> or SwissDock<sup>33</sup>.

### Protein preparation

The modelled receptor was processed for docking studies by deleting crystallographic water molecules with less than three H-bonds. This could also be done manually by editing the .PDB file in a text editor. Next, hydrogen atoms corresponding to neutral pH were added in consideration of ionisation states of amino acids. Following this, coordinates for any missing side-chain atoms were added using Prime v4.0, Schrödinger 2019-2<sup>34</sup>. Finally, the energy of the modelled structure was minimised using the OPLS\_2005 force field<sup>35</sup>. This analysis could also have been performed using open source software such as AutoDock<sup>32</sup>.

## Ligand preparation

The three-dimensional conformations of the 4015 small molecule drugs already in use to treat various diseases and as nutritional supplements were downloaded from the [DrugCentral database](#) and subjected to ligand minimisation using Ligprep (LigPrep, version 2.3, Schrödinger, LLC, New York, NY, 2009). This analysis could also have been performed using open source software such as AutoDock<sup>32</sup>. The compounds were minimised by assigning force field OPLS\_2005 and stereoisomers were calculated after retaining specific chiralities. The absorption, distribution, metabolism and excretion (ADME) predictions were performed for all ligands using the QikProp package<sup>36</sup>. This analysis could also have been performed using open source software such as SWISS-ADME<sup>37</sup>.

## Molecular docking

The active site on the prepared receptor was defined around the selected residues (Arg426, Tyr436, Pro462, Thr486, Gly488, and Tyr491) with a 10Å radius. This generated a grid box measuring 20X20X20Å. The docking of small molecules over SARS-CoV-2-S was performed using Glide v7.8. This analysis could also have been performed using open source software such as AutoDock<sup>32</sup>. Schrödinger 2019-2<sup>38</sup> in different modes sequentially with defined and incremental precision, and computational time differences. The best-docked conformer with minimum Glide energy and E model energy was selected and lowest-energy docked complex of three known molecules streptomycin, ciprofloxacin, and glycyrrhizic acid (GA) in complex with SARS-CoV-2-S were selected for molecular dynamic simulations.

## Molecular dynamics (MD) simulations

The MD<sup>39</sup> of shortlisted complexes were studied using the OPLS\_2005 force field<sup>40</sup> in a plane TIP3P water model<sup>41</sup>. MD simulations were performed using Desmond version 4.2<sup>42</sup>. This analysis could also have been performed using open source software such as GROMACS<sup>43</sup>. The system was built by dissolving the streptomycin/SARS-CoV-2-S, ciprofloxacin/SARS-CoV-2-S, and GA/SARS-CoV-2-S complexes in an orthorhombic box containing water molecules, allowing a buffer region of 10Å between atoms and box peripherals. The system was further minimised using the L-BFGS algorithm for a minimum of 10 steepest descent steps and a maximum of 2000 iterations until a gradient threshold of 25 kcal/mol/Å and convergence threshold of 1.0 kcal/mol/Å was reached. For short-range electrostatic interactions, the solid-phase

microextraction<sup>44</sup> method was employed at 1e-09 tolerance and 9Å cut-off radius. The built systems were gradually warmed up to 300K in the NPT ensemble with a time step of 2fs. A 100ns MD simulation in the NPT ensemble was performed using a Nose-Hoover thermostat<sup>40</sup>. Resulting root mean square deviation (RMSD) and root mean square fluctuation (RMSF) values were analysed.

## Results and discussion

### Multiple sequence alignment of complete genomes

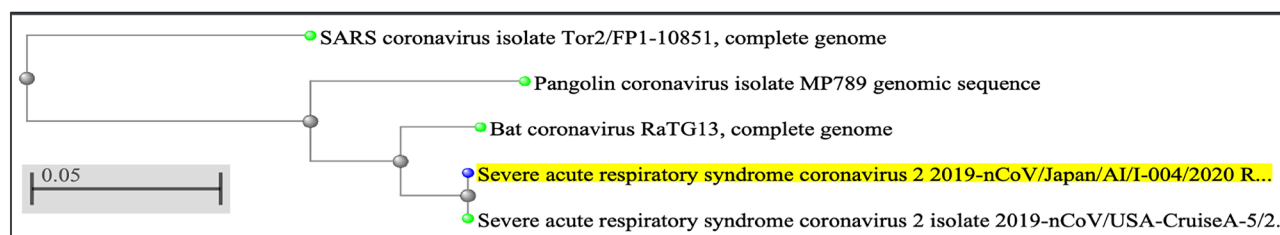
The complete genome of coronavirus SARS-CoV-2, Bat coronavirus RaTG13, Pangolin coronavirus isolate MP789, and SARS-CoV obtained as BLAST hits were aligned and a phylogenetic tree was constructed ([Figure 1](#)).

The MSA demonstrated the molecular similarities between the organisms. RaTG13 has been identified as a neighbour genome for SARS-CoV-2 and this justifies the hypothesis that the infection may be transmitted from bats. Meanwhile, the subsequent neighbours were Pangolin MP789 and SARS-CoV. This preliminary sequence alignment enabled the understanding of sequence similarities and evolutionary information, which is deeply fundamental to the process of drug discovery.

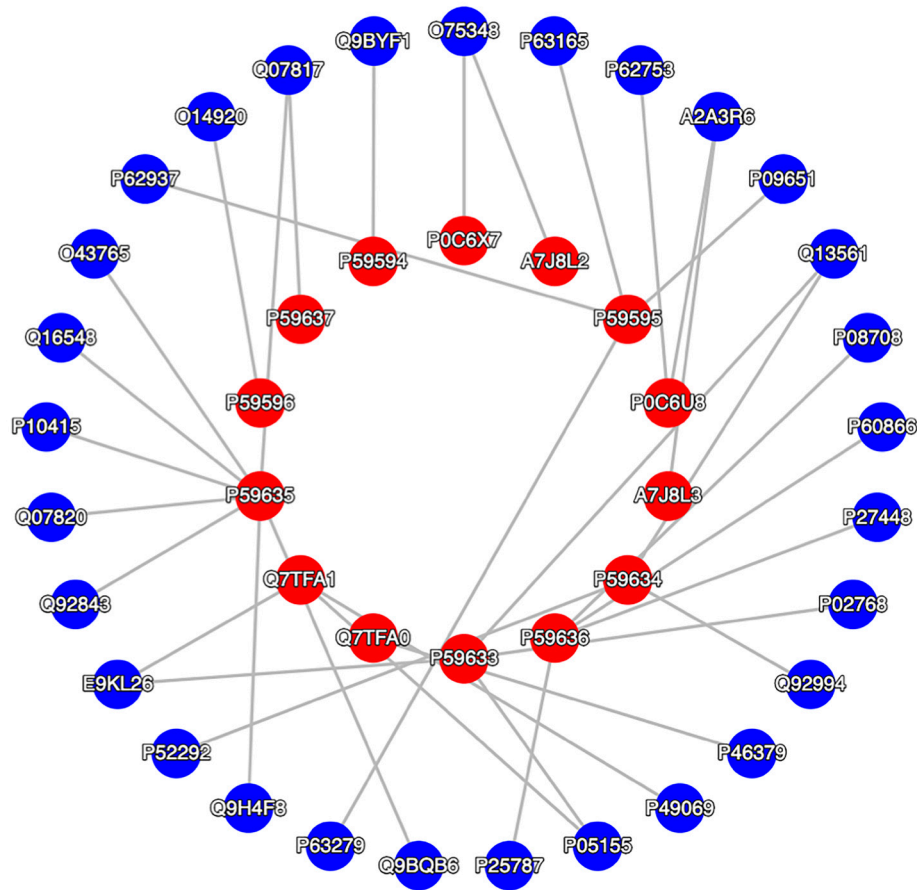
### Topological analysis and target validation

A detailed investigation of the pathogen-host interactome can shed clear insights on the mechanism of viral infection and the pathology involved. Due to a lack of interaction data on SARS-CoV-2, the SARS-CoV proteome was considered and the SARS-CoV/human interactome was built by screening domain interactions between SARS-CoV/human protein-protein interactions, and then the network distribution, topological and functional analyses were performed ([Figure 2](#)). The circular shapes correspond to proteins (nodes) which are labelled by Uniprot\_IDs and details about the nodes are listed in [Table 1](#).

Among 14 proteins of SARS-CoV, the majority of SARS-CoV/human interaction involves five non-structural proteins (NS3B, NS6, NS7A, NS7B and NS8A with four, three, eight, three and one human proteins, respectively), three open reading frame (ORF) polyproteins (ORF9B, A7J8L3 and A7J8L2 with four, one and one human proteins, respectively), two replicase proteins (R1A and R1AB with two and one human proteins, respectively), the Membrane protein (VME1 with human IKKB), Envelope membrane protein (VEMP with human B2CL1), Nucleoprotein (NCAP with four human proteins) and Spike



**Figure 1.** Cladogram constructed using neighbour joining tree construction method, depicting the distance between the complete genome sequences subjected for multiple sequence alignment. This figure was generated using EMBL-EBI Clustal Omega.



**Figure 2.** The SARS-CoV/human pathogen-host interactome illustrating the protein-protein interactions between proteins. The 28 blue nodes correspond to human proteins and 14 red nodes are SARS-CoV-2 proteins. The nodes are connected by 35 edges. This figure was generated using Pathogen-Host Interaction Search Tool (PHISTO).

**Table 1.** The list of proteins involved in SARS-CoV/human interactions with experimental methods and Pubmed ID as reference.

| Uniprot ID | Pathogen protein | Uniprot ID | Human protein | Experimental method                | Pubmed ID |
|------------|------------------|------------|---------------|------------------------------------|-----------|
| P59596     | VME1             | O14920     | IKKB          | Coimmunoprecipitation              | 17705188  |
| P59637     | VEMP             | Q07817     | B2CL1         | Coimmunoprecipitation              | 16048439  |
| P59637     | VEMP             | Q07817     | B2CL1         | Other Methods                      | 16048439  |
| P59594     | SPIKE            | Q9BYF1     | ACE2          | Experimental interaction detection | 18343844  |
| P59594     | SPIKE            | Q9BYF1     | ACE2          | Pull down                          | 23486063  |
| P0C6U8     | R1A              | P62753     | RS6           | Anti tag coimmunoprecipitation     | 19838190  |
| P0C6U8     | R1A              | A2A3R6     | A2A3R6        | Anti tag coimmunoprecipitation     | 19838190  |
| P0C6X7     | R1AB             | O75348     | VATG1         | Anti bait coimmunoprecipitation    | 16226257  |
| P0C6X7     | R1AB             | O75348     | VATG1         | Anti tag coimmunoprecipitation     | 16226257  |
| P0C6X7     | R1AB             | O75348     | VATG1         | Experimental interaction detection | 16226257  |
| P0C6X7     | R1AB             | O75348     | VATG1         | Phage display                      | 16226257  |
| P0C6X7     | R1AB             | O75348     | VATG1         | ELISA                              | 16226257  |
| P59636     | ORF9B            | P08708     | RS17          | Two hybrid                         | 22046132  |

| Uniprot ID | Pathogen protein | Uniprot ID | Human protein | Experimental method            | Pubmed ID |
|------------|------------------|------------|---------------|--------------------------------|-----------|
| P59636     | ORF9B            | P60866     | RS20          | Two hybrid                     | 22046132  |
| P59636     | ORF9B            | P27448     | MARK3         | Two hybrid                     | 22046132  |
| P59636     | ORF9B            | P25787     | PSA2          | Two hybrid                     | 22046132  |
| P59636     | ORF9B            | P25787     | PSA2          | LUMIER                         | 22046132  |
| P59636     | ORF9B            | P27448     | MARK3         | LUMIER                         | 22046132  |
| P59636     | ORF9B            | P60866     | RS20          | LUMIER                         | 22046132  |
| P59636     | ORF9B            | P08708     | RS17          | LUMIER                         | 22046132  |
| Q7TFA0     | NS8A             | P46379     | BAG6          | Two hybrid                     | 22046132  |
| Q7TFA0     | NS8A             | P46379     | BAG6          | LUMIER                         | 22046132  |
| Q7TFA1     | NS7B             | P49069     | CAMLG         | Two hybrid                     | 22046132  |
| Q7TFA1     | NS7B             | P05155     | IC1           | Two hybrid                     | 22046132  |
| Q7TFA1     | NS7B             | E9KL26     | E9KL26        | Two hybrid                     | 22046132  |
| Q7TFA1     | NS7B             | P05155     | IC1           | LUMIER                         | 22046132  |
| Q7TFA1     | NS7B             | P49069     | CAMLG         | LUMIER                         | 22046132  |
| Q7TFA1     | NS7B             | E9KL26     | E9KL26        | LUMIER                         | 22046132  |
| P59635     | NS7A             | Q9BQB6     | VKOR1         | Two hybrid                     | 22046132  |
| P59635     | NS7A             | Q9H4F8     | SMOC1         | Two hybrid                     | 22046132  |
| P59635     | NS7A             | Q92843     | B2CL2         | Coimmunoprecipitation          | 17428862  |
| P59635     | NS7A             | Q07820     | MCL1          | Coimmunoprecipitation          | 17428862  |
| P59635     | NS7A             | P10415     | BCL2          | Coimmunoprecipitation          | 17428862  |
| P59635     | NS7A             | Q16548     | B2LA1         | Coimmunoprecipitation          | 17428862  |
| P59635     | NS7A             | O43765     | SGTA          | Coimmunoprecipitation          | 16580632  |
| P59635     | NS7A             | Q07817     | B2CL1         | Coimmunoprecipitation          | 17428862  |
| P59635     | NS7A             | Q9BQB6     | VKOR1         | LUMIER                         | 22046132  |
| P59635     | NS7A             | Q9H4F8     | SMOC1         | LUMIER                         | 22046132  |
| P59635     | NS7A             | O43765     | SGTA          | Other Methods                  | 16580632  |
| P59634     | NS6              | Q13561     | DCTN2         | Two hybrid                     | 22046132  |
| P59634     | NS6              | Q92994     | TF3B          | Two hybrid                     | 22046132  |
| P59634     | NS6              | P52292     | IMA1          | Two hybrid                     | 17596301  |
| P59634     | NS6              | Q13561     | DCTN2         | LUMIER                         | 22046132  |
| P59634     | NS6              | Q92994     | TF3B          | LUMIER                         | 22046132  |
| P59633     | NS3B             | Q13561     | DCTN2         | Two hybrid                     | 22046132  |
| P59633     | NS3B             | P02768     | ALBU          | Two hybrid                     | 22046132  |
| P59633     | NS3B             | P05155     | IC1           | Two hybrid                     | 22046132  |
| P59633     | NS3B             | E9KL26     | E9KL26        | Two hybrid                     | 22046132  |
| P59633     | NS3B             | P05155     | IC1           | LUMIER                         | 22046132  |
| P59633     | NS3B             | Q13561     | DCTN2         | LUMIER                         | 22046132  |
| P59633     | NS3B             | P02768     | ALBU          | LUMIER                         | 22046132  |
| P59633     | NS3B             | E9KL26     | E9KL26        | LUMIER                         | 22046132  |
| P59595     | NCAP             | P63165     | SUMO1         | Anti tag coimmunoprecipitation | 15848177  |
| P59595     | NCAP             | P09651     | ROA1          | Two hybrid                     | 15862300  |
| P59595     | NCAP             | P63279     | UBC9          | Two hybrid                     | 16998888  |
| P59595     | NCAP             | P63279     | UBC9          | Coimmunoprecipitation          | 16998888  |
| P59595     | NCAP             | P63165     | SUMO1         | Coimmunoprecipitation          | 15848177  |

| Uniprot ID | Pathogen protein | Uniprot ID | Human protein | Experimental method                | Pubmed ID |
|------------|------------------|------------|---------------|------------------------------------|-----------|
| P59595     | NCAP             | P62937     | PPIA          | Coimmunoprecipitation              | 15688292  |
| P59595     | NCAP             | P09651     | ROA1          | Pull down                          | 15862300  |
| P59595     | NCAP             | P09651     | ROA1          | Surface plasmon resonance          | 15862300  |
| P59595     | NCAP             | P62937     | PPIA          | Surface plasmon resonance          | 15688292  |
| P59595     | NCAP             | P63279     | UBC9          | Other Methods                      | 16998888  |
| P59595     | NCAP             | P63279     | UBC9          | Other Methods                      | 17037517  |
| P59595     | NCAP             | P09651     | ROA1          | Other Methods                      | 15862300  |
| A7J8L3     | A7J8L3           | A2A3R6     | A2A3R6        | Anti tag coimmunoprecipitation     | 19838190  |
| A7J8L2     | A7J8L2           | O75348     | VATG1         | Anti bait coimmunoprecipitation    | 16226257  |
| A7J8L2     | A7J8L2           | O75348     | VATG1         | Anti tag coimmunoprecipitation     | 16226257  |
| A7J8L2     | A7J8L2           | O75348     | VATG1         | Experimental interaction detection | 16226257  |
| A7J8L2     | A7J8L2           | O75348     | VATG1         | Phage display                      | 16226257  |
| A7J8L2     | A7J8L2           | O75348     | VATG1         | ELISA                              | 16226257  |

LUMIER, luminescence-based mammalian interactome mapping; ELISA, enzyme-linked immunosorbent assay.

glycoprotein (SPIKE with human ACE2). With these observations, we determine the high specificity of Membrane, Envelope and Spike glycoprotein interactions with the host through specific entry points. Hence, these three SARS-CoV proteins can be a potential target to inhibit the pathogen-host interaction specifically, while other interactions are more versatile. To ensure the impact of inhibition of IKKB, B2CL1, and ACE2 mediated interaction, the landscape of the SARS-CoV/human interaction was further analysed for degree and betweenness centrality distributions of the host, as shown in [Table 2](#).

The degree of connectivity estimates the number of directly connecting neighbours to a particular node, while betweenness centrality estimates the frequency of nodes occurring on the shortest paths in the context of other nodes. In the protein interactomes, a node with a high degree of connectivity is identified as hub protein and a node with maximum betweenness centrality is identified as bottleneck protein. In the current topological analysis, the node with the lowest degree of distribution 1 and betweenness centrality 0.0 was A2A3R6. However, the molecular function of A2A3R6 (Uniprot ID: [A2A3R6](#)) is not well understood in both human physiology or pathology. Hence, ACE2, with the degree of distribution 4 and betweenness centrality 2271, was the next most significant node, as shown in [Figure 3](#), and it was identified as a key node or key player in the SARS-CoV/host interaction. Hence, the SARS-CoV-S interaction with host ACE2 was identified as a potential drug target. As information about the SARS-CoV-2/human interaction is not available, the SARS-CoV/human interaction data was used. We studied the similarity between SARS-CoV and SARS-CoV-2 by sequence analysis and RBD prediction.

### Sequence analysis and RBD predictions

As depicted in [Figure 4](#), the alignment between the S-protein of SARS-CoV-2 and that of Bat coronavirus RaTG13 was closer than with the S-protein of SARS-CoV. The alignment at RBD

site residues 317 to 569 was found to be more than 80% similar to SARS-CoV and RaTG13, particularly at major residues including Tyr436, Thr486, Gly488 and Tyr491 but excluding Arg426 and Pro462, as shown in [Figure 5](#). Considering the evolution, the available elucidated structure of the SARS-CoV/ACE2 complex (PDB ID: [6CS2](#)) was used as a template for homology modelling.

The residues involved in the interaction of SARS-CoV with ACE2 were predicted using the Prime module available in Schrodinger Small Molecule Suite and the major interactions are tabulated in [Table 3](#) and shown in [Figure 6](#). A very strong interaction was seen between the smallest amino acid, Gly488, with Lys353, Gly354, and Asp355. This interaction is facilitated by two features; one hydrogen bond and 94.9% buried solvent accessible surface area. Remaining residues also showed significantly strong interactions with ACE2. Hence, the same residues were made centric to generate the grid.

### Homology modelling and validation of SARS-CoV-2-S protein

The modelling of SARS-CoV-2 was performed using the crystal structure of SARS-CoV-S as a template, which was 97% identical to the query. The modelled protein shown in [Figure 7A](#) was validated for quality and preparedness. The Ramachandran plot generated using the protein preparation wizard confirmed the quality of modelled structure by plotting >95% residues in the allowed region, as shown in [Figure 7B](#).

### Molecular docking of small molecules with SARS-CoV-2-S

The repurposing of small molecules as therapeutics to treat COVID-19 requires knowledge of the interaction of the therapeutic molecule with SARS-CoV-2-S. Initial high-throughput virtual screening suggested 142 molecules that exhibit reasonable interaction with SARS-CoV-2-S. Following this, the shortlisted molecules were docked in SP mode where the accuracy of prediction was improved. The docking in SP mode suggested 15 top

**Table 2. Topological analysis of the human proteins and of the human proteins targeted by SARS-CoV in the human interactome.** Cumulative degree and betweenness centrality distributions.

| Sl.No | Human Uniprot ID | Human protein | Degree | Betweenness centrality |
|-------|------------------|---------------|--------|------------------------|
| 1     | A2A3R6           | A2A3R6        | 1      | 0.0                    |
| 2     | Q9BYF1           | ACE2          | 4      | 2271.0                 |
| 3     | Q9H4F8           | SMOC1         | 4      | 115.53                 |
| 4     | Q9BQB6           | VKOR1         | 8      | 4431.9                 |
| 5     | P49069           | CAMLG         | 11     | 3788.8                 |
| 6     | P05155           | IC1           | 13     | 8518.7                 |
| 7     | O75348           | VATG1         | 15     | 17898.0                |
| 8     | Q16548           | B2LA1         | 15     | 10821.0                |
| 9     | Q92994           | TF3B          | 19     | 7621.0                 |
| 10    | Q92843           | B2CL2         | 20     | 12060.0                |
| 11    | P08708           | RS17          | 24     | 15475.0                |
| 12    | Q07820           | MCL1          | 35     | 23003.0                |
| 13    | Q13561           | DCTN2         | 44     | 32832.0                |
| 14    | P27448           | MARK3         | 49     | 32544.0                |
| 15    | P62937           | PPIA          | 57     | 90417.0                |
| 16    | P25787           | PSA2          | 68     | 26732.0                |
| 17    | Q07817           | B2CL1         | 84     | 113360.0               |
| 18    | P10415           | BCL2          | 97     | 171060.0               |
| 19    | O43765           | SGTA          | 133    | 545880.0               |
| 20    | O14920           | IKKB          | 134    | 99858.0                |
| 21    | P52292           | IMA1          | 143    | 310540.0               |
| 22    | P63165           | SUMO1         | 164    | 334120.0               |
| 23    | P60866           | RS20          | 170    | 37806.0                |
| 24    | P09651           | ROA1          | 174    | 176900.0               |
| 25    | P02768           | ALBU          | 178    | 735080.0               |
| 26    | P46379           | BAG6          | 205    | 684320.0               |
| 27    | P62753           | RS6           | 238    | 67566.0                |
| 28    | P63279           | UBC9          | 252    | 817850.0               |

molecules, listed in Table 4 as lead molecules. As hydroxychloroquine has been identified as a possible treatment for COVID-19, it was also subjected to subsequent docking in XP mode. All 15 molecules showed better interaction than hydroxychloroquine with SARS-CoV-2-S. The three molecules streptomycin, ciprofloxacin, and GA had low interaction penalties and displayed better interactions with the ACE2 binding site on the RBD of SARS-CoV-2-S, as shown in Figure 8A–C, respectively. The three molecules were selected based on their reported anti-viral activity, safety, availability, and affordability<sup>45–47</sup>.

For SARS-CoV-2-S, the Glide generated docking model showed that streptomycin could bind to SARS-CoV-2-S in a

manner highly similar to the SARS-CoV-2-S and ACE2 interaction. The binding pocket of streptomycin was in the RBD site, which has been observed to be an acceptor for ACE2. Streptomycin was well-fitted with the shape of the pocket, as shown in Figure 8A and Figure 9A, with an XP score of -6.5, where it formed a total five hydrogen bonds, among which two hydrogen bonds were formed by donating electrons from N31 and N32 atoms to the Glu493 side-chain atoms. Simultaneously, two other hydrogen bonds were observed between the backbone atoms of Leu501 by receiving electrons from hydroxyl groups at the 5th and 6th carbon atoms of the S1 six-carbon ring of streptomycin. The remaining H-bonds were formed between the backbone atom of Ser503 and the hydroxyl group at the 6th carbon atom at the G3 group of streptomycin. However, the stability of the interaction cannot be pronounced without molecular dynamic simulations.

The docking model of ciprofloxacin illustrated its binding mode on the RBD site, which has been observed to be a key interference site for virus-host interaction. The ciprofloxacin fit with reasonable steric complementarity into the RBD pocket, as shown in Figure 8B and Figure 9B, with an XP score of -5.31. The interaction of ciprofloxacin with SARS-CoV-2-S was facilitated by two hydrogen bonds between Val492 and Phe499; each bond being formed by receiving and donating electrons from hydroxyl and ketone groups, respectively.

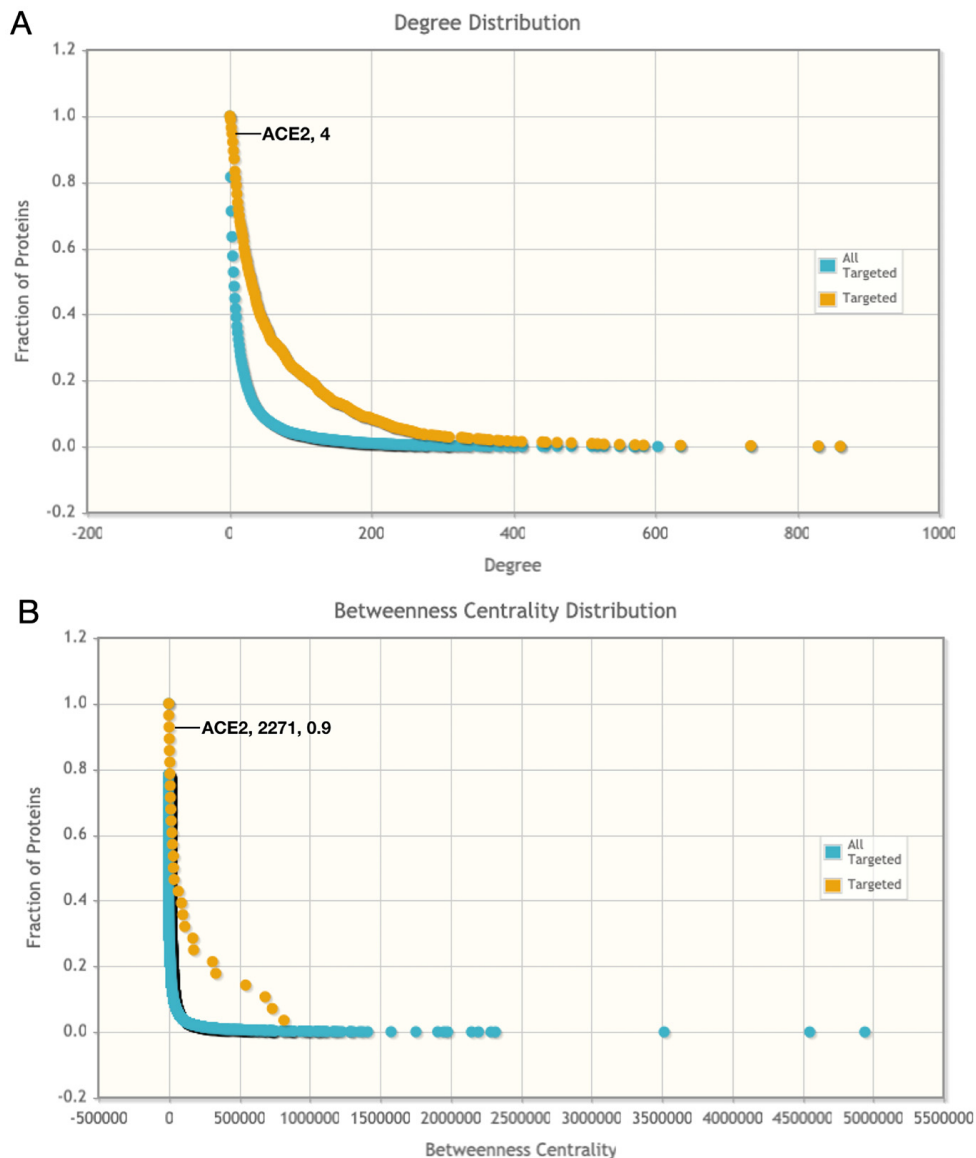
The docking model of GA illustrated its binding mode on the RBD site, which has been observed to be a key site for interference of the virus-host interaction. The GA fit with steric complementarity in the RBD pocket, as shown in Figure 8C and Figure 9C, with an XP score of -7.474. The docking of GA with SARS-CoV-2-S was facilitated by three hydrogen bonds with Leu464, Val492, and Glu493 by receiving electrons from the hydroxyl groups of GA. Additionally, the ketone group of GA formed a hydrogen bond, with the backbone atoms of Phe499 receiving the electrons.

#### Molecular dynamics simulation of protein-ligand complex

As the SARS-CoV-2-S receptor has 1273aa, it requires enormous computational time to perform MD simulation for the whole range of protein, hence, we confined this study only to the RBD portion, ranging from 317th residue to 569th residue, for MD Simulation.

**RMSD analysis of protein-ligand complex.** The RMSD can illustrate the average difference in the displacement of selected atoms in a particular frame compared to its reference frame. The plots in Figure 10 illustrate the evolution of a protein (left Y-axis) and ligand (right Y-axis) RMSD. Post simulation, the protein and ligand frames are initially aligned over the backbone atom coordinates of the reference frame, and then the RMSD is extrapolated. The information on protein-ligand RMSD can dissect and demonstrate the conformational differences that occurred throughout the simulation. The RMSD of between 1–3 Å is fairly acceptable for small, globular proteins. An RMSD exceeding this indicates a major conformational change during the simulation and pronounces the instability of the complex.





**Figure 3. Cumulative degree and betweenness centrality distributions among host proteins involved in the SARS-CoV interaction.** Host proteins that are targeted by SARS-CoV have an approximate degree and betweenness centrality. **A)** Degree distribution highlighting ACE2 position and **B)** betweenness centrality distribution highlighting ACE2 position. These findings are statistically significant by the Fligner-Killeen (median) test. This figure was generated using Pathogen-Host Interaction Search Tool (PHISTO).

The RMSD plot for the streptomycin/SARS-CoV-2-S complex, shown in Figure 10A, attained equilibrium at 5ns and thereafter showed stability with a maximum RMSD of 1 Å (peaks of 2.5 Å - 3.0 Å) up to 55ns. After 55ns a change in the equilibrium state was observed. However, the RMSD was within 1.5 Å, which is acceptable. Similarly, the streptomycin RMSD (right Y-axis) was observed to be significantly higher than the RMSD of the receptor at the RBD site. Thus, it is likely that streptomycin diffuses from its initial binding site after 48ns.

The RMSD plot for the ciprofloxacin/SARS-CoV-2-S complex, shown in Figure 10B, attained equilibrium at 2ns and thereafter

showed stability with a maximum RMSD of 1.8 Å (peaks of 2.4 Å - 4.2 Å) up to 58ns. After 58ns a sudden change in equilibrium state was observed. However, the RMSD was within 2 Å, which is acceptable. On the other hand, the RMSD values for ciprofloxacin were observed to be significantly in alignment with the RMSD of SARS-CoV-2-S at the RBD site. Thus, it is likely that ciprofloxacin can retain its initial binding site up to 100ns.

The RMSD plot for the GA/SARS-CoV-2-S complex, shown in Figure 10C, attained equilibrium until 100ns. Compared to SARS-CoV-2-S complexes with streptomycin and ciprofloxacin, it was found that the SARS-CoV-2-S complex with GA was





**Figure 5.** Aligned region of S-protein from SARS\_CoV-2, SARS-CoV and RatG13 to understand the conservation of amino acids at the receptor-binding domain region as generated using EMBL-EBI Clustal Omega.

**Table 3.** List of residues involved in SARS-CoV-ACE2 interaction. The residues with hydrogen bonding, better surface complementarity and buried SASA are tabulated and a few other weak interactions are ignored.

| Residue          | Closest   | Distance | Interactions                                 | # HB | # SB | # vWC | SC   | B_SASA |
|------------------|-----------|----------|--|------|------|-------|------|--------|
| <b>B:426:Arg</b> | D:329:Glu | 2.7 A    | 2x hb, 1x salt bridge, 1x clash to D:329:Glu | 2    | 1    | 1     | 0.43 | 72.0%  |
| <b>B:436:Tyr</b> | D:38:Asp  | 3.2 A    | 1x hb to D:38:Asp                            | 1    | 0    | 0     | 0.75 | 36.9%  |
|                  | D:42:Gln  | 3.2 A    |  |      |      |       |      |        |
| <b>B:462:Pro</b> | D:19:Ser  | 2.8 A    | 1x hb to D:19:Ser                            | 1    | 0    | 0     | 0.73 | 87.3%  |
|                  | D:24:Gln  | 3.7 A    |  |      |      |       |      |        |
| <b>B:486:Thr</b> | D:41:Tyr  | 2.8 A    | 1x hb to D:41:Tyr                            | 1    | 0    | 0     | 0.87 | 79.8%  |
|                  | D:330:Asn | 2.9 A    |  |      |      |       |      |        |
|                  | D:355:Asp | 3.1 A    |  |      |      |       |      |        |
|                  | D:357:Arg | 3.8 A    |  |      |      |       |      |        |
| <b>B:488:Gly</b> | D:353:Lys | 3.0 A    | 1x hb to D:353:Lys                           | 1    | 0    | 0     | 0.65 | 94.9%  |
|                  | D:354:Gly | 3.9 A    |  |      |      |       |      |        |
|                  | D:355:Asp | 4.0 A    |  |      |      |       |      |        |
| <b>B:491:Tyr</b> | D:353:Lys | 3.2 A    |  | 0    | 0    | 0     | 0.85 | 70.0%  |
|                  | D:354:Gly | 3.6 A    |  |      |      |       |      |        |
|                  | D:393:Arg | 3.7 A    |  |      |      |       |      |        |

HB, hydrogen bond; DS, disulfides, vWC, van der Waals clash; SC, surface complementarity; B\_SASA, buried solvent accessible surface area (SASA).

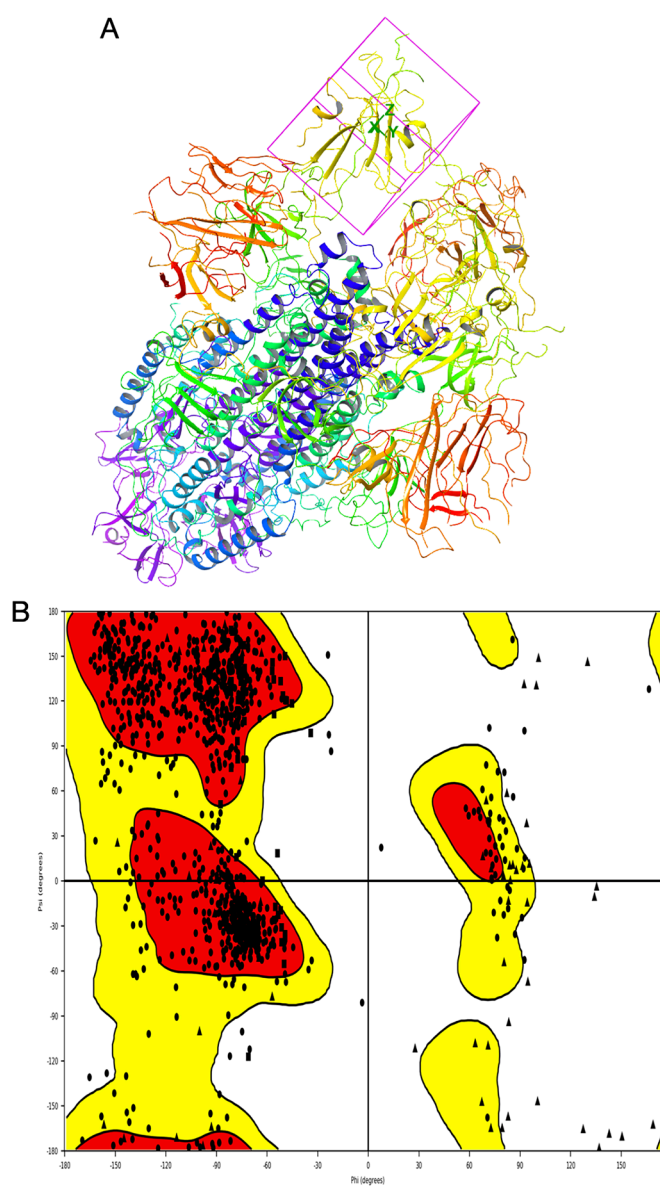
stable until the end of the simulation without any drift in equilibrium. On the other hand, the RMSD values for GA were observed to be significantly in alignment with the RMSD of the SARS-CoV-2-S RBD domain in almost all the frames. Hence, it is likely that it remains in its initial binding site up to 100ns. It is predicted to inhibit SARS-CoV-2-S at the RBD domain comparatively better than streptomycin and ciprofloxacin and

for a longer duration, but its contact with key ligands has to be confirmed through RMSF and protein-ligand contact analysis.

**RMSF analysis.** The RMSF helps characterise minute differences in the protein chain during the simulation. In RMSF plots, peaks correspond to the residues on the protein that fluctuate more during the course of a simulation. Usually, terminals and

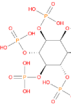
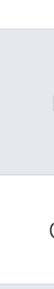
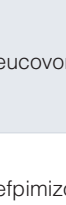
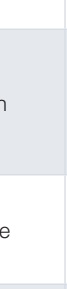
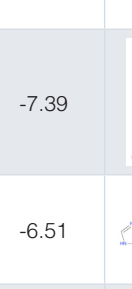
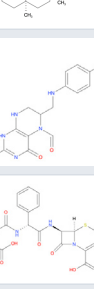

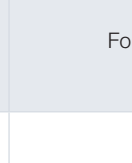
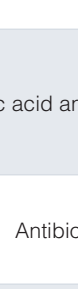
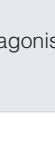
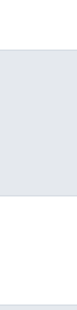
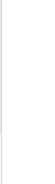



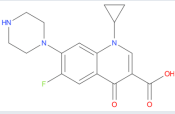
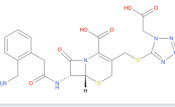
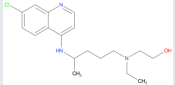
**Figure 6. Amino acids involved in the SARS-CoV B-chain and ACE2 D-chain interaction.** The residues highlighted in blue correspond to the B-Chain of SARS-CoV and residues in green correspond to the ACE2 D-Chain. This figure was generated using Schrodinger's Maestro visualizer. As an alternative, the open source visualizer Python Molecule Viewer (PMV)<sup>48</sup> could also be used.

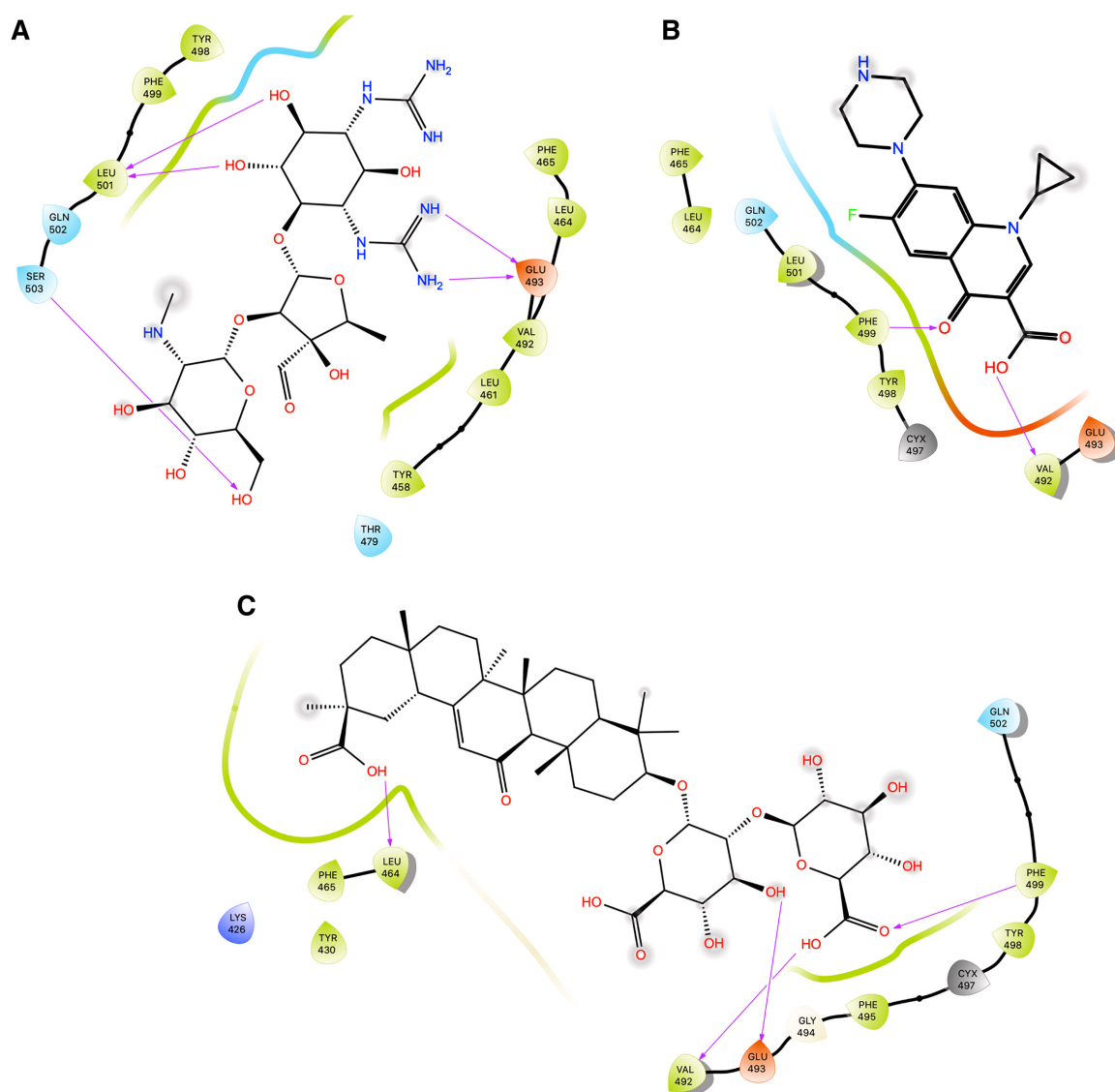


**Figure 7. A)** The modelled structure of SARS-CoV-2 with Arg426, Tyr436, Pro462, Thr486, Gly488 and Tyr491 centric grid box generated for molecular docking, **B)** Ramachandran plot has >95% of amino acids plotted in the allowed region (red and yellow). This figure was generated using Schrodinger's Maestro visualizer. As an alternative, the open source visualizer Python Molecule Viewer (PMV)<sup>48</sup> could also be used.

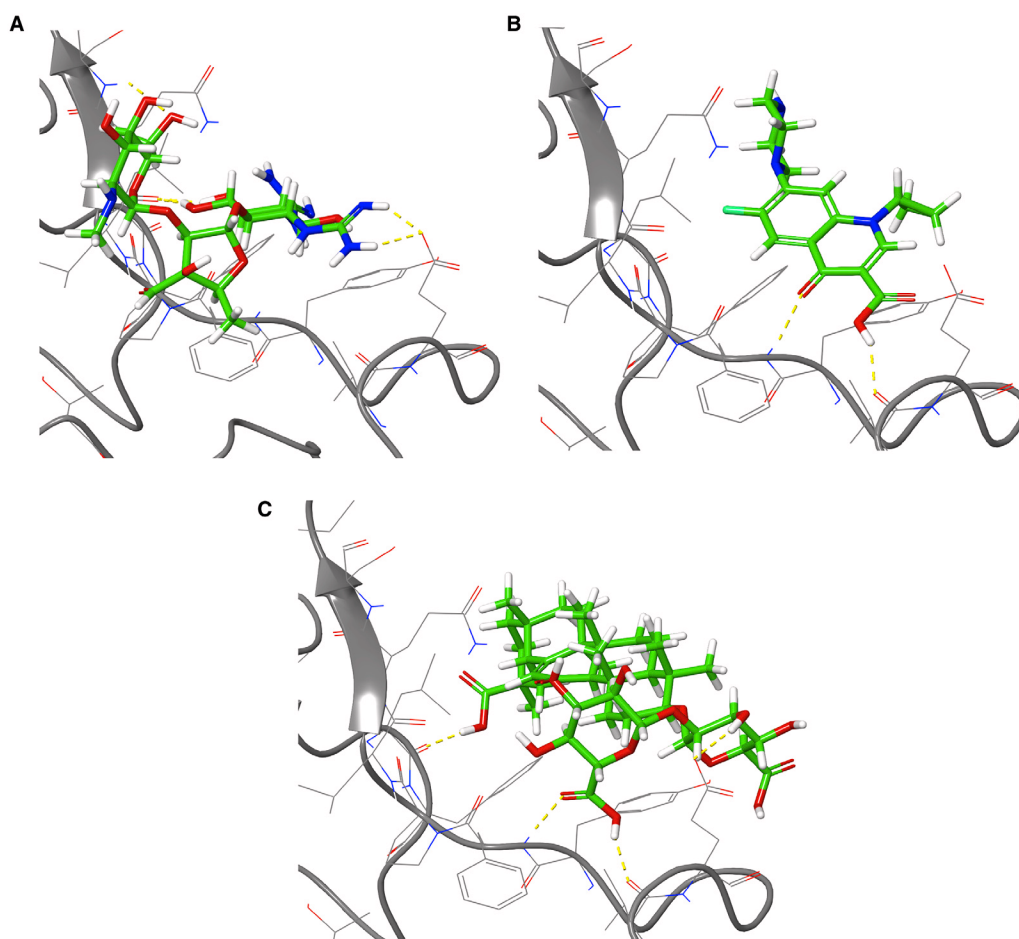
**Table 4.** List of top 15 lead molecules and hydroxychloroquine subjected for molecular docking in XP mode.

| Sl. No | Molecule name     | XP_Score | Mol_Structure  | Pharmacological activity               |
|--------|-------------------|----------|--|--|
| 1      | Fytic acid        | -10.296  |     | Hypocalcemic agent                     |
| 2      | Diquafosol        | -9.109   |    | Purinoreceptor P2Y(2) receptor agonist |
| 3      | Oxiglutatione     | -7.869   |    | Intraocular Irrigating Solution        |
| 4      | Ceftolozane       | -8.07    |    | Antibiotic                             |
| 5      | Glycyrrhizic acid | -7.474   |    | Anti-inflammatory                      |
| 6      | Leucovorin        | -7.39    |    | Folic acid antagonist                  |
| 7      | Cefpimizole       | -6.51    |    | Antibiotic                             |
| 8      | Streptomycin      | -6.509   |   | Antibiotic                             |
| 9      | Ertapenem         | -5.758   |  | Antibiotic                             |
| 10     | Enoxacin          | -5.539   |  | Antibacterial                          |
| 11     | Acetyldigitoxin   | -5.407   |  | Cardioactive                           |
| 12     | Pefloxacin        | -5.399   |  | Antibacterial                          |
| 13     | Faropenem         | -5.354   |  | Antibiotic                             |

| Sl. No | Molecule name      | XP_Score | Mol_Structure   | Pharmacological activity |
|--------|--------------------|----------|---|--------------------------|
| 14     | Ciprofloxacin      | -5.318   |  | Antibacterial            |
| 15     | Ceforanide         | -5.302   |  | Antibiotic               |
| 16     | Hydroxychloroquine | -5.302   |  | Antimalarial             |



**Figure 8. Two-dimensional (2D) illustration of the small molecule interaction in the ACE2 binding site of the receptor-binding domain of SARS-CoV-2-S. A)** Interaction of streptomycin facilitated by five H-bonds, shown as pink arrows. **B)** Interaction of ciprofloxacin facilitated by two H-bonds, shown as pink arrows. **C)** Interaction of glycyrrhizic acid, facilitated by seven H-bonds, shown as pink arrows. This figure was generated using Schrodinger's Maestro visualizer. As an alternative, the open source visualizer Python Molecule Viewer (PMV)<sup>48</sup> could also be used.



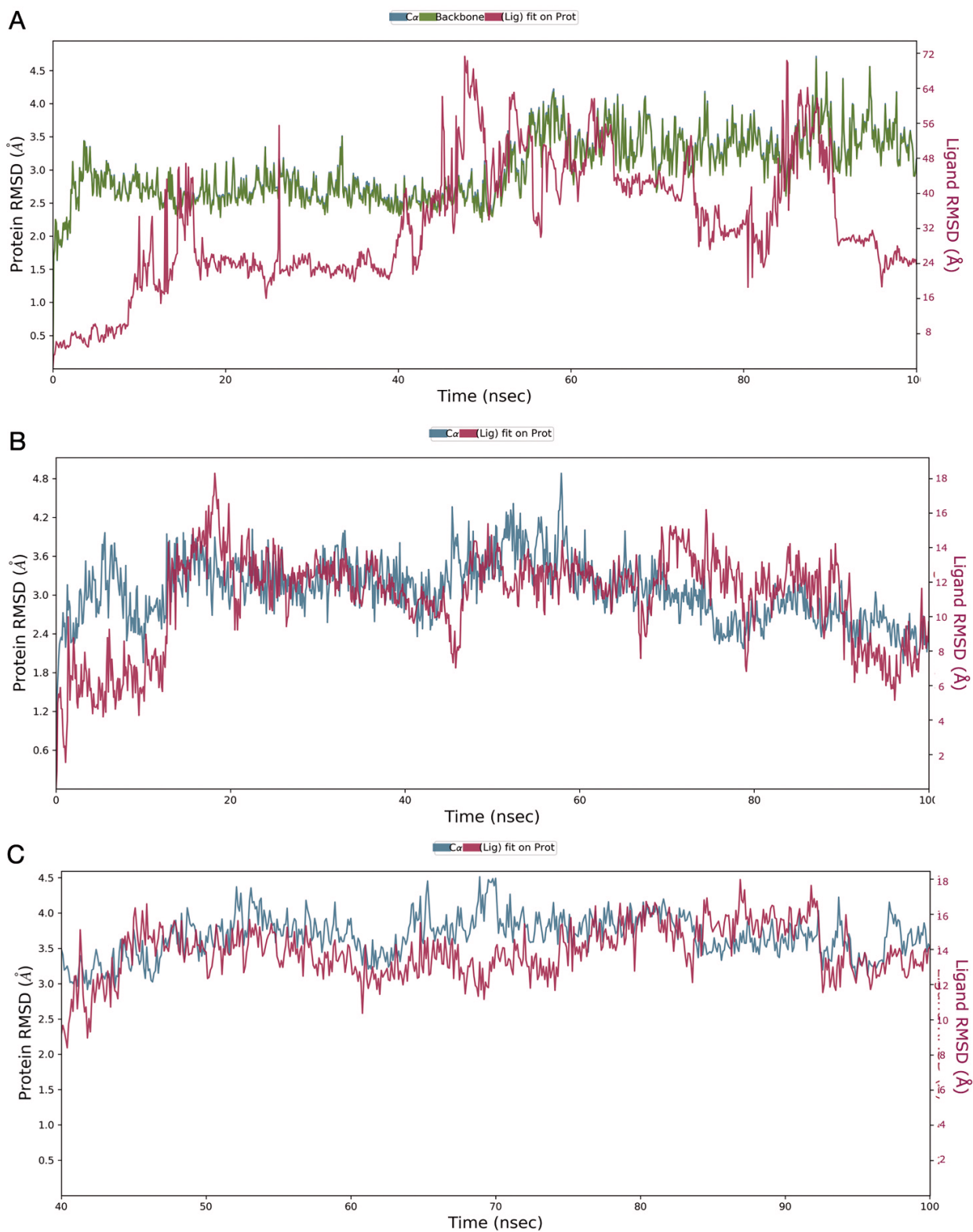
**Figure 9.** Three-dimensional (3D) illustration of the small molecule interaction in the ACE2 binding site of the receptor-binding domain of SARS-CoV-2-S. **A)** Interaction of streptomycin facilitated by five H-bonds. **B)** Interaction of ciprofloxacin facilitated by two H-bonds. **C)** Interaction of glycyrrhizic acid facilitated by five H-bonds. This figure was generated using Schrodinger's Maestro visualizer. As an alternative, the open source visualizer Python Molecule Viewer (PMV)<sup>48</sup> could also be used.

loop regions fluctuate more than other secondary structures like alpha-helices and beta-strands. The secondary structure of the RBD of SARS-CoV-2-S has the same secondary structural elements as the RBD from SARS-CoV, with 74% homologous residues. These residues are majorly formed of loops and are highly flexible. A unique Phe486 residue in the loop plays a key role in ACE2 interaction by occupying a deep hydrophobic pocket in ACE2. In the trimmed RBD structure this loop starts from 148th residue and ends at 172nd residue. Since the ligand-binding site is located in this loop region, a higher RMSD was noticed. In the RMSF plot for the RBD domain of the streptomycin/SARS-CoV-2-S complex, shown in [Figure 11A](#), the RMSF at the loop region was 5.6Å with many ligand contacts (green-coloured vertical bars). This was on par with molecular docking interactions. In the RMSF plot for the RBD domain of the ciprofloxacin/SARS-CoV-2-S complex, shown in [Figure 11B](#), the RMSF at the loop region was 5.6Å with a few ligand contacts (green-coloured vertical bars). This justifies the interactions seen in molecular docking. Further, in the RMSF plot for the RBD domain of the GA/SARS-CoV-2-S complex, shown in

[Figure 11C](#), the RMSF at loop region was 6.3Å with a high number of ligand contacts (green-coloured vertical bars), justifying the interactions seen in molecular docking. Though the ligand contacts are seen in interactions, the simulation time coverage determines their stability.

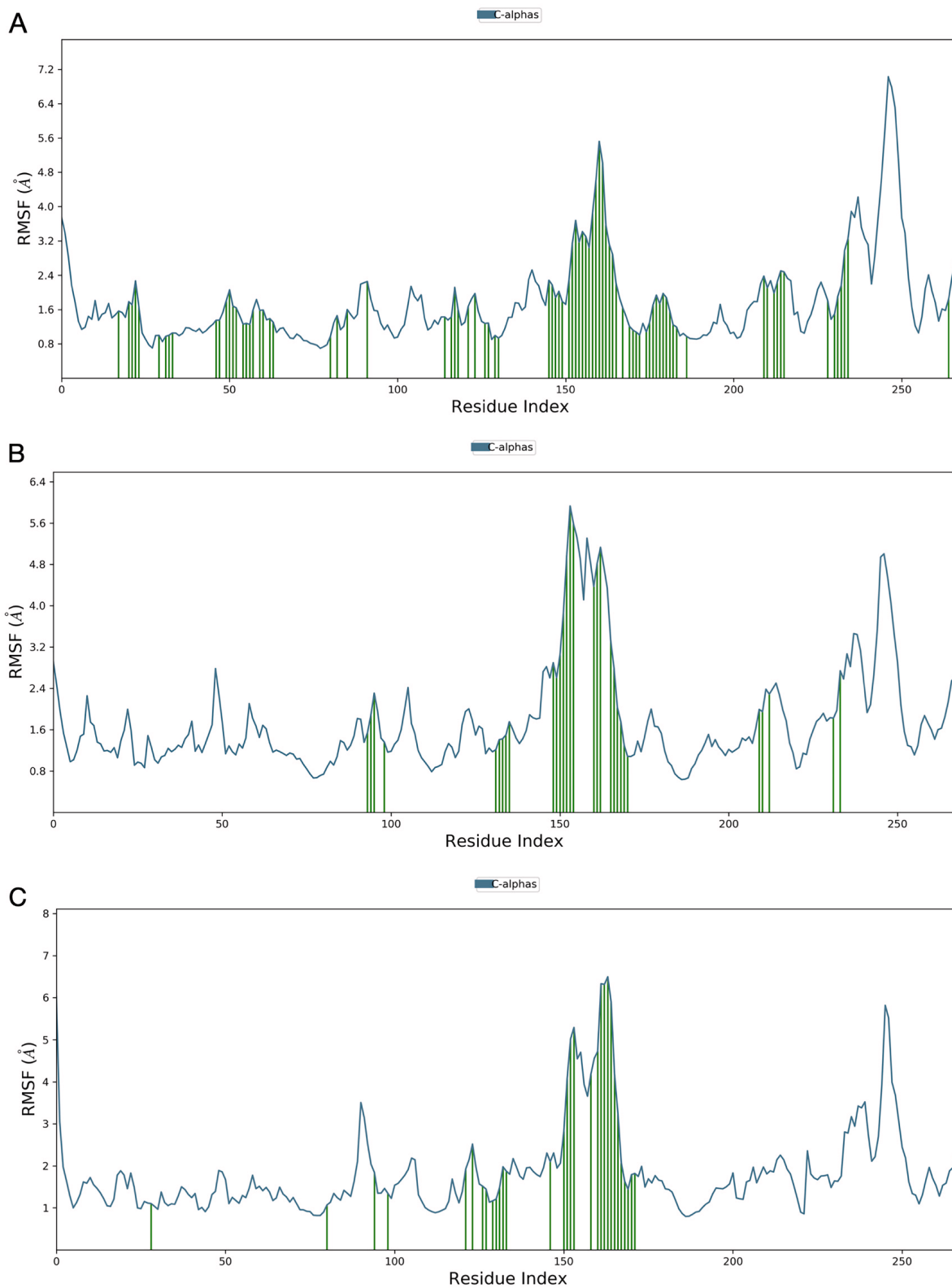
**Protein-ligand contacts.** Protein-ligand interactions can be traced throughout the simulation and can be categorised into four types: hydrogen bonds, hydrophobic, ionic, and water bridges, as summarised in [Figure 12A–12C](#). The stacked bars in the plots are normalised over the course of the trajectory and help us to understand the retention of contact throughout the simulation time. The contacts with a value of more than 0.7 are expected to be retained for over 70% of the total simulation time.

In the protein-ligand contact plot for the streptomycin/SARS-CoV-2-S complex, shown in [Figure 12A](#), residues Glu493 and Lys544 showed maximum interactions fractions, i.e. 0.20 facilitated by hydrogen bonds and water bridges. This suggests that the specific interaction is maintained for 20%



**Figure 10.** The root mean square deviation (RMSD) plot for protein ligand complexes generated after 100 ns molecular dynamics simulation in the NPT ensemble. **A)** streptomycin/SARS-CoV-2-S complex; **B)** ciprofloxacin SARS-CoV-2-S complex; **C)** glycyrrhizic acid/SARS-CoV-2-S complex. This figure was generated using Desmond version 4.2<sup>42</sup>. This analysis could also have been performed using open source software such as GROMACS<sup>43</sup>.





**Figure 11.** The root mean square fluctuation (RMSF) plot for protein ligand complexes generated after 100 ns molecular dynamics simulation in the NPT ensemble. **A)** streptomycin/SARS-CoV-2-S complex; **B)** ciprofloxacin SARS-CoV-2-S complex; **C)** glycyrrhizic acid/SARS-CoV-2-S complex. Desmond version 4.2<sup>42</sup>. This analysis could also have been performed using open source software such as GROMACS<sup>43</sup>.

of the simulation time, and such short interactions are not promising. Hence, streptomycin cannot be a potential inhibitor of SARS-CoV-2-S to offer anti-COVID-19 activity.

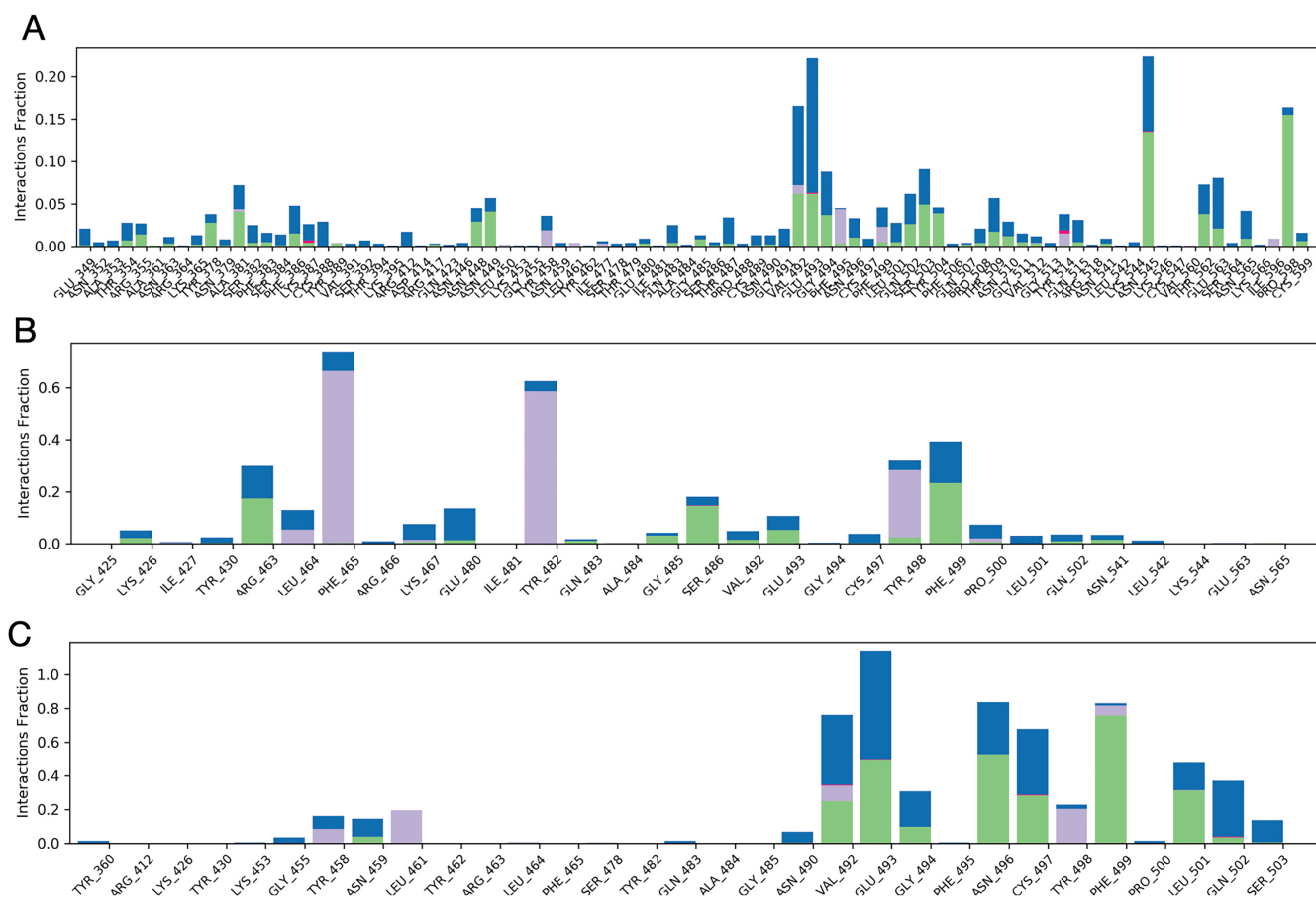
In the protein-ligand contact plot for the ciprofloxacin/SARS-CoV-2-S complex shown in **Figure 12B**, residues Phe465, Tyr482, Tyr498, and Phe499 were seen to have the interactions fractions 0.75, 0.6, 0.35 and 0.39 respectively facilitated by hydrophobic, hydrogen bonds and water bridges. This suggests that for 70%, 60%, 35% and 39% of the simulation time, the specific interaction is maintained by respective residues and such interactions are considered good. Hence, ciprofloxacin may be a potential inhibitor of SARS-CoV-2-S and may offer anti-COVID19 activity.

In the protein-ligand contact plot for the GA/SARS-CoV-2-S complex shown in **Figure 12C**, residues Val492, Glu493, Asn496, Cys497, and Phe499 had the interactions fractions

0.78, 1.12, 0.80, 0.60 and 0.80, respectively, facilitated by hydrophobic, hydrogen bonds and water bridges. This suggests that for 78%, 100%, 80%, 60% and 80% of the simulation time, the specific interaction is maintained by respective residues and such interactions are excellent and promising. Hence, GA can be a potential inhibitor of SARS-CoV-2-S and can offer anti-COVID19 activity.

### Conclusion

Through our topological analysis, we have determined the degree of distribution for viral proteins, and we show that, due to its low degree of distribution, ACE2 is likely to be targeted by viruses like SARS-CoV. Hence, the interaction between the viral protein SARS-CoV-2-S and the host ACE2 receptor is a potential drug target for the repurposing of known drugs. Further, sequence alignment and domain analysis suggest that the RBD is the ligand-binding site. Molecular docking studies have suggested streptomycin, ciprofloxacin, and GA as possible leads to inhibit SARS-CoV-2-S. Molecular dynamic simulation analysis has



**Figure 12. Histogram of protein ligand contacts generated for residues that occur for more than 64.0% of the simulation time in the selected trajectory. A)** streptomycin/SARS-CoV-2-S complex; **B)** ciprofloxacin SARS-CoV-2-S complex; **C)** glycyrrhizic acid/SARS-CoV-2-S complex. Desmond version 4.2<sup>42</sup>. This analysis could also have been performed using open source software such as GROMACS<sup>43</sup>.

indicated that GA is a promising small molecule that could be repurposed as a potential inhibitor of SARS-CoV-2-S to offer anti-COVID19 activity.

## Data availability

All data underlying the results are available as part of the article and no additional source data are required.

## References

- Zhou P, Yang XL, Wang XG, *et al.*: **A pneumonia outbreak associated with a new coronavirus of probable bat origin.** *Nature*. 2020; **579**(7798): 270–273. [PubMed Abstract](#) | [Publisher Full Text](#) | [Free Full Text](#)
- Gorbalenya AE, Baker SC, Baric RS, *et al.*: **Severe acute respiratory syndrome-related coronavirus: The species and its viruses - a statement of the Coronavirus Study Group.** *Nat Microbiol*. 2020. [Publisher Full Text](#)
- World Health Organization: **Clinical management of severe acute respiratory infection when novel coronavirus (CoV) infection is suspected.** [Reference Source](#)
- CDC.** [Reference Source](#)
- FDA.** [Reference Source](#)
- Korea Biomedical Review.** [Reference Source](#)
- Cheng F: **In silico oncology drug repositioning and polypharmacology.** *Methods Mol Biol*. 2019; **1878**: 243–261. [PubMed Abstract](#) | [Publisher Full Text](#)
- Cheng F, Hong H, Yang S, *et al.*: **Individualized network-based drug repositioning infrastructure for precision oncology in the panomics era.** *Brief Bioinform*. 2017; **18**(4): 682–697. [PubMed Abstract](#) | [Publisher Full Text](#)
- Nature Biotechnology.** visited on 20th March. [Reference Source](#)
- Walls AC, Park YJ, Tortorici MA, *et al.*: **Structure, Function, and Antigenicity of the SARS-CoV-2-Spike Glycoprotein.** *Cell*. 2020; 281–292.e6. [PubMed Abstract](#) | [Publisher Full Text](#) | [Free Full Text](#)
- Belouzard S, Chu VC, Whittaker GR: **Activation of the SARS coronavirus spike protein via sequential proteolytic cleavage at two distinct sites.** *Proc Natl Acad Sci U S A*. 2009; **106**(14): 5871–5876. [PubMed Abstract](#) | [Publisher Full Text](#) | [Free Full Text](#)
- Bosch BJ, van der Zee R, de Haan CA, *et al.*: **The coronavirus spike protein is a class I virus fusion protein: structural and functional characterization of the fusion core complex.** *J Virol*. 2003; **77**(16): 8801–8811. [PubMed Abstract](#) | [Publisher Full Text](#) | [Free Full Text](#)
- Burkard C, Verheije MH, Wicht O, *et al.*: **Coronavirus cell entry occurs through the endo-lysosomal pathway in a proteolysis-dependent manner.** *PLoS Pathog*. 2014; **10**(11): e1004502. [PubMed Abstract](#) | [Publisher Full Text](#) | [Free Full Text](#)
- Kirchdoerfer RN, Cottrell CA, Wang N, *et al.*: **Pre-fusion structure of a human coronavirus spike protein.** *Nature*. 2016; **531**(7592): 118–121. [PubMed Abstract](#) | [Publisher Full Text](#) | [Free Full Text](#)
- Millet JK, Whittaker GR: **Host cell entry of Middle East Respiratory Syndrome coronavirus after two-step, furin-mediated activation of the spike protein.** *Proc Natl Acad Sci U S A*. 2014; **111**(42): 15214–15219. [PubMed Abstract](#) | [Publisher Full Text](#) | [Free Full Text](#)
- Millet JK, Whittaker GR: **Host cell proteases: Critical determinants of coronavirus tropism and pathogenesis.** *Virus Res*. 2015; **202**: 120–134. [PubMed Abstract](#) | [Publisher Full Text](#) | [Free Full Text](#)
- Park JE, Li K, Barlan A, *et al.*: **Proteolytic processing of Middle East respiratory syndrome coronavirus spikes expands virus tropism.** *Proc Natl Acad Sci U S A*. 2016; **113**(43): 12262–12267. [PubMed Abstract](#) | [Publisher Full Text](#) | [Free Full Text](#)
- Walls AC, Tortorici MA, Bosch BJ, *et al.*: **Cryo-electron microscopy structure of a coronavirus spike glycoprotein trimer.** *Nature*. 2016; **531**(7592): 114–117. [PubMed Abstract](#) | [Publisher Full Text](#) | [Free Full Text](#)
- Walls AC, Tortorici MA, Frenz B, *et al.*: **Glycan shield and epitope masking of a coronavirus spike protein observed by cryo-electron microscopy.** *Nat Struct Mol Biol*. 2016; **23**(10): 899–905. [PubMed Abstract](#) | [Publisher Full Text](#) | [Free Full Text](#)
- Gui M, Song W, Zhou H, *et al.*: **Cryo-electron microscopy structures of the SARS-CoV spike glycoprotein reveal a prerequisite conformational state for receptor binding.** *Cell Res*. 2017; **27**(1): 119–129. [PubMed Abstract](#) | [Publisher Full Text](#) | [Free Full Text](#)
- Kirchdoerfer RN, Cottrell CA, Wang N, *et al.*: **Pre-fusion structure of a human coronavirus spike protein.** *Nature*. 2016; **531**(7592): 118–121. [PubMed Abstract](#) | [Publisher Full Text](#) | [Free Full Text](#)
- Pallesen J, Wang N, Corbett KS, *et al.*: **Immunogenicity and structures of a rationally designed prefusion MERS-CoV spike antigen.** *Proc Natl Acad Sci U S A*. 2017; **114**(35): E7348–E7357. [PubMed Abstract](#) | [Publisher Full Text](#) | [Free Full Text](#)
- Walls AC, Tortorici MA, Snijder J, *et al.*: **Tectonic conformational changes of a coronavirus spike glycoprotein promote membrane fusion.** *Proc Natl Acad Sci U S A*. 2017; **114**(42): 11157–11162. [PubMed Abstract](#) | [Publisher Full Text](#) | [Free Full Text](#)
- Yuan Y, Cao D, Zhang Y, *et al.*: **Cryo-EM structures of MERS-CoV and SARS-CoV spike glycoproteins reveal the dynamic receptor binding domains.** *Nat Commun*. 2017; **8**: 15092. [PubMed Abstract](#) | [Publisher Full Text](#) | [Free Full Text](#)
- Madu IG, Roth SL, Belouzard S, *et al.*: **Characterization of a highly conserved domain within the severe acute respiratory syndrome coronavirus spike protein S2 domain with characteristics of a viral fusion peptide.** *J Virol*. 2009; **83**(15): 7411–7421. [PubMed Abstract](#) | [Publisher Full Text](#) | [Free Full Text](#)
- Heald-Sargent T, Gallagher T: **Ready, Set, Fuse! The Coronavirus Spike Protein and Acquisition of Fusion Competence.** *Viruses*. 2012; **4**(4): 557–580. [PubMed Abstract](#) | [Publisher Full Text](#) | [Free Full Text](#)
- Morris DE, Cleary DW, Clarke SC: **Secondary Bacterial Infections Associated with Influenza Pandemics.** *Front Microbiol*. 2017; **8**: 1041. [PubMed Abstract](#) | [Publisher Full Text](#) | [Free Full Text](#)
- Zhang Z, Schwartz S, Wagner L, *et al.*: **A greedy algorithm for aligning DNA sequences.** *J Comput Biol*. 2000; **7**(1–2): 203–14. [PubMed Abstract](#) | [Publisher Full Text](#)
- Raman K: **Construction and analysis of protein-protein interaction networks.** *Autom Exp*. 2010; **2**(1): 2–10. [PubMed Abstract](#) | [Publisher Full Text](#) | [Free Full Text](#)
- Hwang S, Son SW, Kim SC, *et al.*: **A protein interaction network associated with asthma.** *J Theor Biol*. 2008; **252**(4): 722–731. [PubMed Abstract](#) | [Publisher Full Text](#)
- Sastry, GM, Adzhigirey M, Day T, *et al.*: **Protein and ligand preparation: Parameters, protocols, and influence on virtual screening enrichments.** *J Comput Aid Mol Des*. 2013; **27**(3): 221–234. [PubMed Abstract](#) | [Publisher Full Text](#)
- Morris GM, Huey R, Lindstrom W, *et al.*: **Autodock4 and AutoDockTools4: automated docking with selective receptor flexibility.** *J Comput Chem*. 2009; **30**(16): 2785–91. [PubMed Abstract](#) | [Publisher Full Text](#) | [Free Full Text](#)
- Grosdidier A, Zoete V, Michielin O: **SwissDock, a protein-small molecule docking web service based on EADock DSS.** *Nucleic Acids Res*. 2011; **39**(Web Server issue): W270–W277. [PubMed Abstract](#) | [Publisher Full Text](#) | [Free Full Text](#)
- Jacobson MP, Pincus DL, Rapp CS, *et al.*: **A Hierarchical Approach to All-Atom Protein Loop Prediction.** *Proteins*. 2004; **55**(2): 351–367. [PubMed Abstract](#) | [Publisher Full Text](#)
- Shivakumar D, Williams J, Wu Y, *et al.*: **Prediction of absolute solvation free energies using molecular dynamics free energy perturbation and the OPLS force field.** *J Chem Theory Comput*. 2010; **6**(5): 1509–1519. [PubMed Abstract](#) | [Publisher Full Text](#)
- Dagan-Wiener A, *et al.*: **Bitter or not? BitterPredict, a tool for predicting taste from chemical structure.** *Sci Rep*. 2017; **7**(1): 12074. [PubMed Abstract](#) | [Publisher Full Text](#) | [Free Full Text](#)
- Daina A, Michielin O, Zoete V: **SwissADME: a free web tool to evaluate pharmacokinetics, drug-likeness and medicinal chemistry friendliness of small molecules.** *Sci Rep*. 2017; **7**: 42717. [PubMed Abstract](#) | [Publisher Full Text](#) | [Free Full Text](#)
- Friesner RA, Murphy RB, Repasky MP, *et al.*: **Extra precision glide: docking and scoring incorporating a model of hydrophobic enclosure for protein-ligand complexes.** *J Med Chem*. 2006; **49**(21): 6177–6196. [PubMed Abstract](#) | [Publisher Full Text](#)
- Guo Z, Mohanty U, Noehre J, *et al.*: **Probing the  $\alpha$ -helical structural stability of stapled p53 peptides: molecular dynamics simulations and analysis.** *Chem Biol Drug Des*. 2010; **75**(4): 348–359. [PubMed Abstract](#) | [Publisher Full Text](#)
- Martyna GJ, Klein ML, Tuckerman M: **Nose-Hoover chains-the canonical ensemble via continuous dynamics.** *J Chem Phys*. 1992; **97**(4): 2635–2643. [Publisher Full Text](#)
- Jorgensen WL, Chandrasekhar J: **Comparison of simple potential functions for**

- simulating liquid water.** *J Chem Phys.* 1983; **79**(2): 926–935.  
[Publisher Full Text](#)
42. Bowers KJ, Chow E, Xu H, *et al.*: **Scalable Algorithms for Molecular Dynamics Simulations on Commodity Clusters.** Proceedings of the ACM/IEEE Conference on Supercomputing (SC06), Tampa, Florida, 2006.  
[Reference Source](#)
43. Abraham MJ, Murtola T, Schulz R, *et al.*: **GROMACS: High performance molecular simulations through multi-level parallelism from laptops to supercomputers.** *SoftwareX.* 2015; **1-2**: 19–25.  
[Publisher Full Text](#)
44. Essmann U, Perera L, Berkowitz ML, *et al.*: **A smooth particle mesh Ewald method.** *J Chem Phys.* 1995; **103**: 8577–8593.  
[Publisher Full Text](#)
45. Thomas DB, Susan OW: **Streptomycin as an Antiviral Agent: Mode of Action.** *Science.* 1963; **141**(3585): 1065–1067.  
[PubMed Abstract](#) | [Publisher Full Text](#)
46. Ilaria U, Elena A, Francesca T, *et al.*: **Possible Antiviral Effect of Ciprofloxacin Treatment on Polyomavirus BK Replication and Analysis of Non-Coding Control Region Sequences.** *Virology.* 2013; **10**: 274.  
[PubMed Abstract](#) | [Publisher Full Text](#) | [Free Full Text](#)
47. Pompei P, Pani A, Flore O, *et al.*: **Antiviral activity of glycyrrhizic acid.** *Experientia.* 1980; **36**(3): 304.  
[PubMed Abstract](#) | [Publisher Full Text](#)
48. Sanner MF: **Python: A Programming Language for Software Integration and Development.** *J Mol Graph Model.* 1999; **17**(1): 57–61.  
[PubMed Abstract](#)

# Open Peer Review

Current Peer Review Status:  

Version 1

Reviewer Report 27 July 2020

<https://doi.org/10.5256/f1000research.26631.r67868>

© 2020 HL R. This is an open access peer review report distributed under the terms of the [Creative Commons Attribution License](#), which permits unrestricted use, distribution, and reproduction in any medium, provided the original work is properly cited.



**Raghavendra HL** 

College of Medical and Health Sciences, Wollega University, Nekemte, Ethiopia

The manuscript entitled “*In silico* screening of known small molecules to bind ACE2 specific RBD on Spike glycoprotein of SARS-CoV-2 for repurposing against COVID-19” addresses the repurposability of known drugs against COVID-19. Spike glycoprotein is the most popular drug target for SARS-CoV-2 having a significant role in host entry. With this basic understanding, the manuscript is reviewed and the observations are listed below.

- Abstract: Conclusion:

The statement “Hence, the molecules screened for inhibitory properties against SARS-CoV-2-S can be clinically used to treat COVID-19 since the safety profile is already known.” can be rewritten as “The GA of plant origin shown superior interaction with SARS-CoV-2-S compared to rest other molecules, hence, GA can be clinically investigated to confirm its efficacy to treat COVID-19.”

- Methods: Homology modelling of SARS-CoV-2-S protein

The crystal structure of SARS-CoV-S and ACE2 complex (PDB ID: 6ACD) is used as a template for homology modelling. It is expected to discuss the identity, query coverage between the query and template. Discuss the criteria for template selection.

- In the figure legend for Figures 8c, 9c, 10c, 11c, and 12c glycyrrhizic acid can be replaced by GA. The manuscript can be accepted for indexing with above-mentioned changes.

## References

1. BR B, Damle H, Ganju S, Damle L: In silico screening of known small molecules to bind ACE2 specific RBD on Spike glycoprotein of SARS-CoV-2 for repurposing against COVID-19. *F1000Research*. 2020; **9**. [Publisher Full Text](#)

**Is the work clearly and accurately presented and does it cite the current literature?**

Yes

**Is the study design appropriate and is the work technically sound?**

Yes

**Are sufficient details of methods and analysis provided to allow replication by others?**

Yes

**If applicable, is the statistical analysis and its interpretation appropriate?**

Yes

**Are all the source data underlying the results available to ensure full reproducibility?**

Yes

**Are the conclusions drawn adequately supported by the results?**

Yes

**Competing Interests:** No competing interests were disclosed.

**Reviewer Expertise:** Gestational Diabetes Mellitus, Omics, Drug Discovery, Phytopharmacology and Bioinformatics

**I confirm that I have read this submission and believe that I have an appropriate level of expertise to confirm that it is of an acceptable scientific standard.**

Reviewer Report 14 July 2020

<https://doi.org/10.5256/f1000research.26631.r66947>

© 2020 Vidya S. This is an open access peer review report distributed under the terms of the [Creative Commons Attribution License](#), which permits unrestricted use, distribution, and reproduction in any medium, provided the original work is properly cited.



**S.M. Vidya**

Department of Biotechnology, NMAM Institute of Technology, Udipi, Karnataka, India

In the present study authors have made an effort to repurpose the known drugs against SARS-CoV-2. Although the study is well organized and presented, a few minor changes are suggested for betterment.

1. The name of the molecules should begin with Uppercase.
2. In an abstract, authors have mentioned about the anti-viral activity of streptomycin, ciprofloxacin, and glycyrrhizic acid. But, it requires the literature support. Authors can cite the references for the anti-viral/ ant-microbial activity in Methods section.
3. In Results and Discussions, authors could claim the better affinity of glycyrrhizic acid towards SARS-CoV-2-S in comparison with other two molecules. Change suggested: Additionally, the ketone group of GA formed a hydrogen bond, with the backbone atoms of Phe499 receiving the electrons and possess the better affinity towards SARS-CoV-2-S when compared to Streptomycin and Ciprofloxacin.
4. In conclusion section, authors have mentioned that, ACE2 is likely to be targeted by viruses like SARS-CoV. Since, authors have tabulated the methods and references for ACE2 and SARS-CoV spike protein interaction in table 1, it is better to rewrite as "ACE2 is known to be targeted by viruses like SARS-CoV".

**Is the work clearly and accurately presented and does it cite the current literature?**

Yes

**Is the study design appropriate and is the work technically sound?**

Yes

**Are sufficient details of methods and analysis provided to allow replication by others?**

Yes

**If applicable, is the statistical analysis and its interpretation appropriate?**

Not applicable

**Are all the source data underlying the results available to ensure full reproducibility?**

Yes

**Are the conclusions drawn adequately supported by the results?**

Yes

**Competing Interests:** No competing interests were disclosed.

**Reviewer Expertise:** Phytochemical screening, Pharmacology, Molecular docking

**I confirm that I have read this submission and believe that I have an appropriate level of expertise to confirm that it is of an acceptable scientific standard.**

---

The benefits of publishing with F1000Research:

- Your article is published within days, with no editorial bias
- You can publish traditional articles, null/negative results, case reports, data notes and more
- The peer review process is transparent and collaborative
- Your article is indexed in PubMed after passing peer review
- Dedicated customer support at every stage

For pre-submission enquiries, contact [research@f1000.com](mailto:research@f1000.com)

**F1000Research**